THE JOURNAL OF PHYSICAL CHEMISTRY C

Article

pubs.acs.org/JPCC

^{127}I and ^{207}Pb Solid-State NMR Spectroscopy and Nuclear Spin Relaxation in PbI_2: A Preliminary Study

R. E. Taylor,[†] Peter A. Beckmann,[‡] Shi Bai,[§] and C. Dybowski*[,§]

[†]Department of Chemistry and Biochemistry, University of California, Los Angeles, Los Angeles, California 90095-1569, United States

[‡]Department of Physics, Bryn Mawr College, Bryn Mawr, Pennsylvania 19010-2899, United States

[§]Department of Chemistry and Biochemistry, University of Delaware, Newark, Delaware 19716-2522, United States

ABSTRACT: Lead iodide is a layered structure that experiences polytypism. The 2H polytype contains high rates of iodine vacancies but retains its stoichiometry. This characteristic feature makes it potentially useful for many practical applications. The hopping of iodine ions among vacancies is the dominant motion in the 2H polytype. We present a preliminary ^{127}I and ^{207}Pb solid-state nuclear magnetic resonance (NMR) spectroscopy and spin−lattice relaxation study of the 2H polytype below 400 K. We present reasonable models for the solid-state NMR results in terms of the effects of iodine hopping and lattice vibrations.

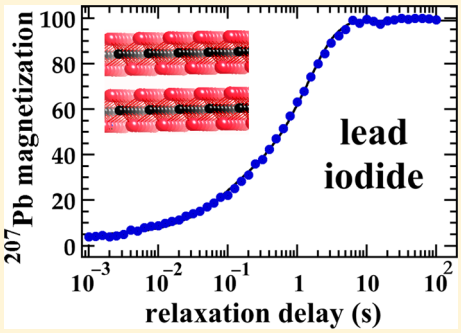

1. INTRODUCTION

Lead iodide (PbI_2) has unusual structural properties[1] that result in interesting physical and electronic properties which make this ionic conductor/semiconductor[2] a candidate for use in a variety of applications (see section 2).[2−7] Despite many published reports using a variety of experimental probes,[2−37] the dynamics of the lead and iodine ions at the atomic level are not well understood. Techniques such as X-ray diffraction[38] and neutron scattering provide static information at the atomic level.[10,13,20,23,25,39] Techniques such as conductivity measurements[4,5,10,11,14,16,18,22,28,29,32,34] give macroscopic information, where the dynamics of atoms can only be described by nonunique models. Although descriptions of atomic motion in this material are model-dependent, ^{207}Pb and ^{127}I nuclear magnetic resonance (NMR) experiments can considerably reduce the range of potentially successful models. We present possible interpretations of NMR data in terms of the effects of iodine hopping and lattice vibrations on the time-dependent NMR spin−lattice mechanisms. Although a single definitive model for the motion is not available yet, this preliminary study points the way for other laboratories, with multifrequency solid-state NMR capabilities, to refine these models.

Sample preparation and thermal history are very important in these systems. As a result, solid-state NMR measurements, which are particularly sensitive to structure at the atomic level, can be difficult to reproduce. Many reports using other techniques provide seemingly contradictory results and consequently different models for ionic dynamics that may depend on the sample preparation. We have taken care to analyze materials that have been as well-characterized as possible, but there is still some sample-to-sample variability.

Solid-state NMR spectroscopy provides insight into the electronic and geometric structures of molecules and solids as well as average dynamical properties.[40] NMR-based structural information is primarily derived from an analysis of the line shape due to the chemical-shift interaction, the direct dipole−dipole interaction with other spins including electrons, and/or the quadrupolar interaction (for cases where a nucleus has a spin quantum number $I > 1/2$).[40] NMR-based information on dynamics is obtained from nuclear spin−lattice relaxation studies as a function of temperature and NMR frequency (which is proportional to the applied magnetic field) in the solid state[40] or from the effects of motion on the spectroscopic line shape.

NMR investigations of heavy-metal-containing solids are frequently challenging because of the very wide resonance lines and often long spin−lattice relaxation times.[41] Theoretical predictions of NMR properties of heavy-metal-containing solids are challenging because the electrons in heavy atoms must be treated relativistically.[42−44]

In this paper, we investigate the temperature dependence of the ^{207}Pb and ^{127}I solid-state NMR spectra and spin−lattice relaxation rates of PbI_2 to gain insight into the relationship between the *structure* and the *dynamics* in this technologically important material.

Received: March 7, 2014
Revised: April 11, 2014
Published: April 11, 2014

dx.doi.org/10.1021/jp5023423 | *J. Phys. Chem. C* 2014, 118, 9143−9153

2. A BRIEF REVIEW OF THE PROPERTIES OF, AND SELECTIVE PREVIOUS WORK ON, LEAD IODIDE

Lead iodide (PbI_2) is an ionic semiconductor[2] useful in a variety of applications from image recording[7] to room-temperature photocells, X-ray detectors, and low-energy γ-ray detectors.[3−6] The applications depend strongly on the nature of the structure and the resulting dynamics. In addition, the propensity toward cluster formation[21,26] and for taking up molecules in its layered structure has led to the study of the intercalation of molecules,[12,8,39] the study of colloidal nanoparticle suspensions,[6,27] and the development of nanobelt bundles.[13] Quantum wells of different sizes can be formed from it[9] as well as quantum dots in solution.[21]

Many uses are traceable to the structural variability of PbI_2 that allows subtle variation of properties. In the solid, each Pb atom is surrounded by six iodine atoms in a *nearly* octahedral $[PbI_6]^{-4}$ unit.[1,23,45] The stacking of layers of these clusters produces slightly distorted hexagonal close-packed (HCP) or rhombohedral close-packed (RCP) layered structures.[1,45] The structure is characterized by strong ionic-like bonding within the I−Pb−I "sandwich" and weaker van der Waals-like bonding between the layers.[1,23] The Pb−I distance is 0.322 nm, the I−Pb−I layer is approximately 0.7 nm thick, the distance between I atoms in neighboring sandwiches is 0.42 nm, and the distance between adjacent I−I planes in different sandwiches is 0.35 nm.[1] (As a reference, the I−I distance in gaseous I_2 is 0.27 nm[20] and the Pb−Pb distance in the pure Pb metal is 0.35 nm.[15] These two values give a radius of the iodine atom of approximately 0.14 nm and a radius of the Pb atom of approximately 0.18 nm.) The reported melting point is 675 K, and the reported boiling point is 1145 K.[41] The density of PbI_2 depends on the details of the structure and on the vacancy rate; it ranges from 5.0 to 6.2 g cm^{-3}.[23]

The stacking arrangements of the structures produce polytypism in solid PbI_2 and many polytypes are known.[1] These are labeled 2H, 4H, 12R, etc., depending on the stacking. The letter refers to hexagonal (H) close packing or rhombohedral (R) close packing, and the number is twice the number of I−Pb−I sandwiches in the unit cell. The structures of the 2H and 4H polytypes are shown in Figure 1 in terms of the ABC hexagonal close-packing arrangement of atoms. The 2H polytype requires one sandwich to characterize the repeating unit (Figure 1b), the 4H polytype requires two sandwiches (Figure 1c), and the 12R polytype (not shown) requires six sandwiches. Studies show that the lattice constants for the various polytypes of PbI_2 are identical within ±0.1 pm.[1,25] The 2H polytype is the stable form at room temperature. It has the property, central to this study, that only 80% of the atomic sites are occupied, at least in samples prepared in some ways,[23] and it retains its ideal crystal structure, even though the vacancy rate is 20%.[23] This high vacancy rate has been confirmed by comparison of the experimentally measured density with the calculated crystallographic density.[23]

A reversible transition between the 2H polytype (Figure 1a,b) and the 4H polytype (Figure 1c) or the 12R polytype occurs in the vicinity of 400 K.[31,33] There is a range of transition temperatures in the literature, and this probably reflects different preparations and/or thermal histories. One study[25] found a 2H−12R first-order transition near 367 K with an enthalpy change of ~0.28 kJ mol^{-1} and an activation energy of 3.8 eV (366 kJ mol^{-1}) for the processes associated with the

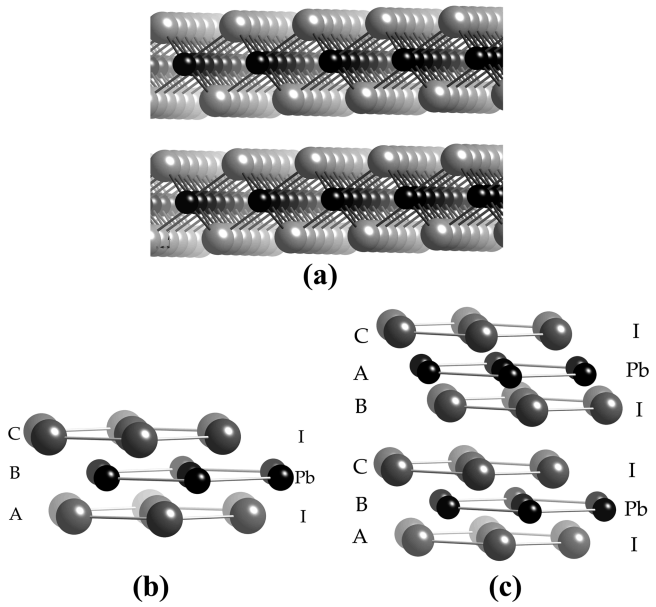

Figure 1. Idealized structures of the 2H and 4H polytypes of PbI_2. The smaller black spheres are Pb atoms, and the larger gray spheres are I atoms. Depth perception is used for clarity and atoms "farther into the page" appear lighter. The lines joining atoms are "guides for the eye" and are not intended to imply bonding. (a, b) The 2H polytype. Atom coordinates from the Inorganic Crystal Structure Database (ICSD), reference #068819 which, in turn, are from ref 23. The real structures have a 20% vacancy rate. The view in (a) results from a rotation of 6° about an axis in the *xy*-plane (perpendicular to the Pb and I planes) from the 110 plane. In (b) the ABC structure of the 2H polytype is shown, and I and Pb rows are labeled. (c) ABCBAC structure of the 4H polytype. Atom coordinates from ICSD 024263 which, in turn, are from ref 37. These figures are adapted from Figures 1, 3, and 4 in ref 1.

kinetics of this phase change.[25] This enthalpy of transition is quite small, only about 5% that of melting solid water. These processes probably involve transitions of the low-temperature 2H polytype to the higher-temperature 4H or 12R polytype.

The high atomic vacancy rate in lead iodide crystals (ca. 20%), while maintaining the PbI_2 stoichiometry,[23] should not be confused with defects induced in the PbI_2 crystal by photodecomposition, where metallic lead is produced with loss of iodine.[29] The high vacancy rate promotes ionic conduction within the PbI_2 crystal, with iodine conduction dominant below 540 K and lead conduction dominant above 540 K.[34] Although predominantly an ionic conductor, lead iodide also displays electronic conduction characteristic of a wide-band semiconductor with a band gap of approximately 2.4 eV (0.23 MJ mol^{-1}).[2,5]

The conductivity of lead iodide has been the subject of numerous investigations.[4,5,10,11,14,16,18,22,28,29,32,34] A study of the temperature dependence of the capacitance and loss tangent[5] indicates the presence of two thermally activated processes affecting its electrical response. The first process, with an activation energy of 0.087 eV (8.4 kJ/mol), is in the range of 288−348 K, and the second process, with a reported activation energy of 0.23 eV (22 kJ/mol), is dominant in the range of 348−393 K. These energies are very much smaller than the ionization energy of 10.45 eV (1.008 MJ/mol).[41]

3. EXPERIMENTAL METHODS

The ^{127}I and ^{207}Pb solid-state NMR data were acquired at three magnetic field strengths. Studies with Bruker Avance

dx.doi.org/10.1021/jp5023423 | J. Phys. Chem. C 2014, 118, 9143−9153

spectrometers in a magnetic field of 7.05 T were carried out at the University of California, Los Angeles (UCLA), and at the University of Delaware (UD). At this field strength, the ^{207}Pb NMR frequency is 62.79 MHz and the ^{127}I NMR frequency is 60.05 MHz. Studies were also carried out in a magnetic field of 11.75 T with a Bruker Avance spectrometer at UD. At 11.75 T, the ^{207}Pb frequency is 104.63 MHz and the ^{127}I frequency is 100.06 MHz. A few ^{207}Pb relaxation studies were also carried out at UD at 4.70 T where the ^{207}Pb frequency is 41.86 MHz. The NMR properties of the two nuclei are given in Table 1.

Table 1. NMR Properties of Lead Iodide Nuclei[a]

isotope	spin	natural abundance (%)	magnetogyric ratio (10^7 rad s^{-1} T^{-1})	quadrupolar moment (fm^2)
^{207}Pb	1/2	22.6	5.580 46	n/a
^{127}I	5/2	100	5.389 573	−71.0

[a]From ref 46.

Measurements at 7.05 T were made with a static 5 mm probe and with a 4 mm magic-angle spinning (MAS) probe at UCLA. At UD the samples were examined with a 7 mm MAS probe at 4.70 T and a 4 mm MAS probe at 7.05 and 11.75 T.

Typically, ^{207}Pb data were acquired using a spin−echo sequence $[(\pi/2)_x-\tau-(\pi)_y-\text{acquire}]$, with $\tau = 20$ μs and a ^{207}Pb $\pi/2$ pulse width of 4 μs. The full spin echo was acquired to improve sensitivity. ^{127}I data were acquired using a quadrupolar echo sequence,[47] with a pulse width of 1 μs, which corresponded to the "solid" $\pi/2$ pulse width.[48] All spin−lattice relaxation rate constants were measured by the saturation-recovery technique.[49] At 11.75 T, the relaxation was observed only on the static sample, which showed a single relaxation rate constant. The ^{127}I shift scale (relative to the resonance position of a 0.01 M solution of KI in D_2O) was calibrated using the unified Ξ scale,[46] relating the ^{127}I shift to the ^{1}H resonance of dilute tetramethylsilane in $CDCl_3$ [at a ^{1}H frequency of 300.13 MHz (7.05 T) or at 500.13 MHz (11.75 T)]. The ^{207}Pb NMR data are referenced to the position of the resonance of tetramethyllead at 0 ppm, using static lead nitrate as an external secondary reference.[50] Temperatures were determined from the chemical shift of solid lead nitrate.[50]

4. EXPERIMENTAL RESULTS

4.1. NMR Chemical Shifts and Line Shapes. The static ^{207}Pb NMR line shape of a polycrystalline sample of PbI_2 (Figure 2a) is Gaussian with a full width at half-maximum (fwhm) of 25 ± 1 kHz at a field of 7.05 T. The isotropic ^{207}Pb chemical shift is −31.1 ppm at 7.05 T, in good agreement with the reported value of −29.1 ppm.[41] When the sample is spun at 15 kHz about an axis inclined at the magic angle relative to the 7.05 T magnetic field, the line shape remains Gaussian but becomes narrower, with a fwhm of 20 ± 1 kHz. The center of the line under magic-angle spinning is shifted to −15.1 ppm (Figure 2b). Assuming that the shift is the result of a temperature change (as a consequence of spinning the sample), and using the temperature coefficient of 1.61 ppm/K for PbI_2 (determined below), the 16 ppm shift corresponds to a temperature increase of ∼26 K, in good agreement with the 27.2 K increase measured using lead nitrate being spun at 15 kHz in the same MAS probe.[50]

The interesting result, shown in Figure 2c, is that at the higher magnetic field of 11.75 T, the MAS spectrum shows two

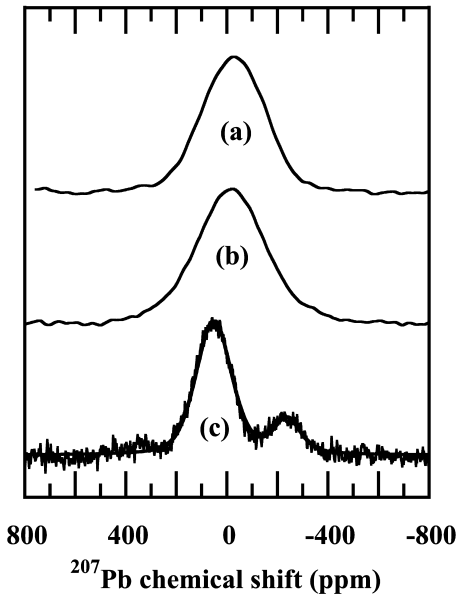

Figure 2. ^{207}Pb spectra of polycrystalline PbI_2: (a) at 7.05 T and room temperature (295 K) without spinning; (b) at 7.05 T and room temperature with MAS at 15 kHz; (c) at 11.75 T and room temperature with MAS at 8 kHz. The fit to the spectrum in (c) is discussed in the text. Taking into account heating as a consequence of spinning, spectrum (b) corresponds to ∼320 K (see text) and spectrum (c) corresponds to a similar temperature. Spectrum (c) was taken using a smaller amount of material.

resolved resonances. At 4.70 and 7.05 T, these two resonances are not resolved, nor are they resolved at 11.75 T without spinning. A fit of this spectrum to the sum of two Gaussian lines (shown as a difficult-to-see solid line in Figure 2c) gives resonances at −236.8 and 55.4 ppm, with an area ratio close to 1:4. Assuming that increased shielding corresponds to increased vacancies, the resonance at −236.8 ppm is assigned to lead nuclei in regions with vacancies and the one at 55.4 ppm to lead nuclei in regions with all sites filled. It is interesting to note that the weighted average of the chemical shifts of the two resonances found in the 11.75 T MAS spectrum is near the average position of the nonspinning single resonance found at either 7.05 or 11.75 T.

The nearly cubic symmetry of the *almost*-octahedral arrangement of iodines[1,45] around the lead center is sufficient to produce a small anisotropy of the ^{207}Pb chemical-shift tensor, the deviation of the chemical-shift span Ω (= $|\delta_{33} - \delta_{11}|$) from zero being indicative of the deviation from perfect octahedral symmetry. The symmetrical structure and the line width of the Gaussian ^{207}Pb resonance indicate that Ω must be no more than 100 ppm (or 6.3 kHz at 7.05 T) (and is probably much smaller) at 295 K, consistent with previous measurements.[24,41] Calculation of the ^{207}Pb NMR parameters of the model $[PbI_6]^{-4}$ unit[45] which include relativistic effects[43,44,51] shows that deviations from octahedral symmetry of less than 1° correspond to spans of something less than 20 ppm. A span of 50 ppm corresponds to a deviation of the I−Pb−I angle from 90° of approximately 3°. Structural reports show that the deviation in the 2H polytype is no more than 0.2°.[1] These facts all suggest that the anisotropy of the Pb powder line shape is close to zero, if not identically zero within the experimental uncertainty of these measurements.

Like a number of other lead-containing materials,[52] the present measurements of the ^{207}Pb isotropic chemical shift δ_{iso}

dx.doi.org/10.1021/jp5023423 | J. Phys. Chem. C 2014, 118, 9143−9153

show a linear dependence on temperature from 220 to 450 K (Figure 3). The temperature coefficient of 1.61 ± 0.02 ppm/K is larger than previously determined coefficients for materials such as lead nitrate, lead molybdate, and lead chloride.[45]

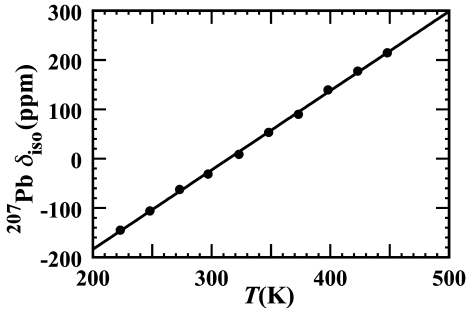

Figure 3. ^{207}Pb isotropic shift δ_{iso} of polycrystalline PbI_2 versus temperature, T, at 7.05 T, determined on a static sample. The line is δ_{iso} = [(1.61 ± 0.02) ppm K^{-1}]T − [505 ± 6 ppm]. Note that the variation of the isotropic shift is continuous through the region from 350 to 450 K, where the phase transition from 2H to either 12R or 4H is expected.

There are six nuclear spin sublevels m_I for the I = 5/2 ^{127}I nucleus. The spectra in Figure 4 show only the central Δm_I 1/2

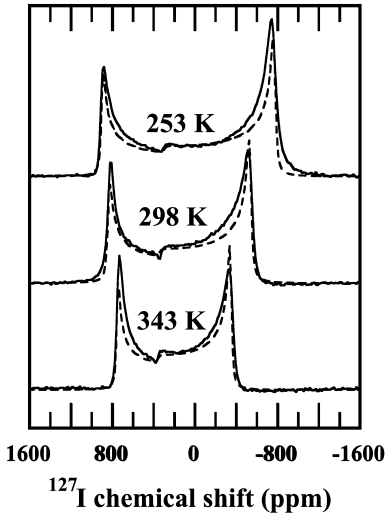

Figure 4. ^{127}I central transition of PbI_2 at 11.75 T at three temperatures. The dashed lines show fits to the experimental data (solid lines).

↔ −1/2 transition of the ^{127}I resonance of polycrystalline PbI_2 at three temperatures at 11.75 T. The line width of the spin-5/2 ^{127}I spectrum narrows as the temperature increases. Simulations[53] of the central-transition line shape are shown in Figure 4, from which the parameters listed in Table 2 are determined using a fitting procedure that assumes the quadrupolar interaction can be treated as a perturbation on the Zeeman interaction with the applied 11.75 T magnetic field.[48] The average ^{127}I quadrupolar coupling constant C_Q decreases linearly with increasing temperature, consistent with dynamic averaging as the lattice librations increase with temperature (Figure 5). The isotropic ^{127}I shift δ_{iso} also varies monotonically

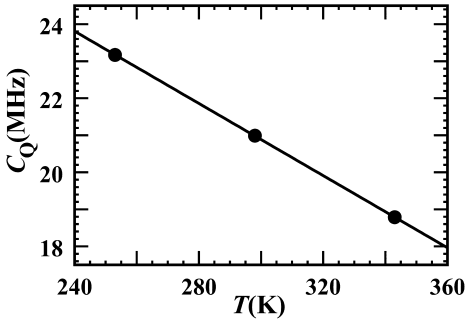

Figure 5. ^{127}I quadrupolar coupling constant C_Q for PbI_2 as a function of temperature, T.

over this range and is approximately linear with temperature (Figure 6). ^{127}I spectra taken at the lower magnetic field of 7.05

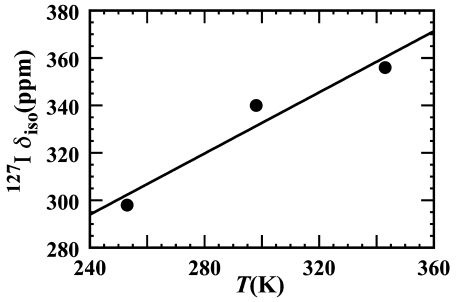

Figure 6. Isotropic chemical shift δ_{iso} of the ^{127}I resonance of PbI_2 as a function of the temperature, T.

T (not shown) are more complex than the 11.75 T spectrum in Figure 4 because the quadrupolar interaction cannot be treated as a small perturbation on the Zeeman interaction at the lower magnetic field, but they similarly show a temperature-dependent line shape that narrows as temperature is increased.

4.2. NMR Spin–Lattice Relaxation Rates. An example of the recovery of the ^{127}I central-transition nuclear magnetization following a perturbation of the central-transition magnetization at 297 K in a field of 7.05 T is shown in Figure 7. In Figure 7, the relaxation delay is the time between the perturbing pulse sequence and the observing pulse sequence that measures the magnetization. About 30% of the central-transition magnet-

Table 2. ^{127}I and ^{207}Pb NMR Parameters of Solid Lead Iodide

nuclear site	T (K)	B (T)	δ_{iso}[c] (ppm)	C_Q (MHz)	υ_Q (MHz)	η_Q	FWHM (kHz)
^{127}I	253	11.75	298[a]	23.173	3.476	0	3.68
^{127}I	298	11.75	340[a]	20.991	3.149	0	2.81
^{127}I	343	11.75	356[a]	18.787	2.818	0	2.17
^{207}Pb	295 (MAS)	7.05	−31.1[b] (−15.1)				25 ± 1 (20 ± 1)

[a]Chemical shifts referenced to the unified Ξ scale (ref 46). [b]Chemical shifts referenced to tetramethyllead by use of lead nitrate as a secondary reference (ref 50). [c]Estimated uncertainty, ±10 ppm.

dx.doi.org/10.1021/jp5023423 | J. Phys. Chem. C 2014, 118, 9143−9153

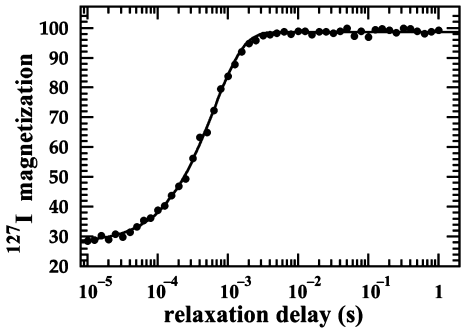

Figure 7. ^{127}I magnetization at 297 K and at 7.05 T versus time following a perturbation that saturates the nuclear magnetization. The full line is a fit to a single-exponential recovery of the magnetization. The time between the saturation pulse sequence and the observing pulse sequence is plotted on a log scale solely for visual clarity.

ization cannot be saturated due to the relatively small T_1 (large relaxation rate R) of the ^{127}I magnetization. The recovery of the central-transition magnetization is, however, well-characterized by a single exponential over the range of temperatures in this study:

$$M(t) = M(\infty)[1 - (1 - \cos\theta)\exp(-Rt)] \quad (1)$$

In these three-parameter fits, $M(\infty)$ is the equilibrium magnetization, R is the relaxation rate constant, and θ is a parameter that characterizes the efficiency of the saturation process. In the ideal case, $\cos\theta = 0$ for a $\theta = 90°$ saturation pulse sequence and $M(0) = 0$. For the ^{127}I relaxation, $\cos\theta \approx 0.3$. The temperature dependence of R is shown in Figure 8. In

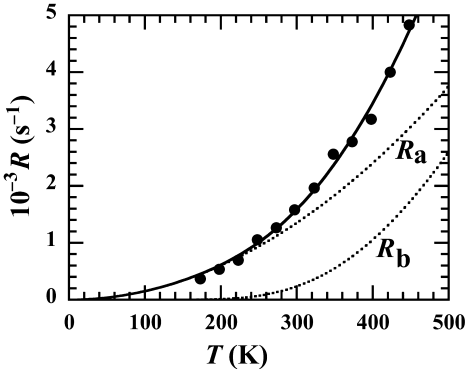

Figure 8. ^{127}I spin−lattice relaxation rate R versus temperature T for static polycrystalline PbI_2 at 7.05 T. The full line is given by eq 4, with the two dotted lines showing the van Kranendonk $R_a \propto T^2$ mechanism and the thermally activated $R_b \propto \exp(-E/kT)$ mechanism.

principle, the recovery of the central-transition magnetization with the pulse sequence used could be nonexponential;[54] however, it appears that the system is in a limit in which the relaxation is at least very close to exponential.

In contrast to the recovery of the iodine magnetization, the recovery of the ^{207}Pb nuclear magnetization in a saturation-recovery experiment at 4.70 and 7.05 T is *not* exponential and is strongly dependent on thermal history. It is probably also dependent on how the lead iodide sample is synthesized and purified since various techniques provide different thermal histories. All the data shown here come from samples purchased from Sigma-Aldrich. They were used as is. It is important to mention that once a sample was taken above approximately 400 K and then back to room temperature, we obtained ^{207}Pb relaxation results at room temperature that were very different from the original room-temperature measurement on the sample. We report rates for samples that had never been taken below 400 K once they had been taken above 400 K. This dependence of the NMR parameters on thermal history may provide a means to investigate thermal history with NMR relaxometry. These relaxation experiments take hours to tens of hours per experiment, and we have not pursued this avenue of investigation here. Figure 9 shows the recovery of the ^{207}Pb

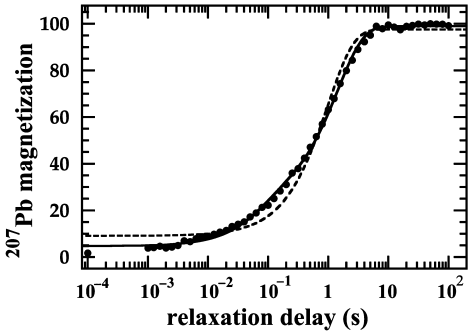

Figure 9. ^{207}Pb magnetization at 295 K and at 7.05 T versus the time following a perturbation that saturates the nuclear magnetization. The full line is either a double-exponential fit or a stretched-exponential fit, the two being indistinguishable at the scale shown. The dashed line is a single-exponential fit. The time between the saturation pulse sequence and the observing pulse sequence is plotted on a log scale solely for visual clarity.

nuclear magnetization at 295 K and 7.05 T. For this spin-1/2 nucleus, the entire nuclear magnetization can be saturated ($\cos\theta \approx 0$). We have confirmed that if only the magnetization data above 30% were used in the fits (to compare the relaxation with the ^{127}I relaxation presented above), the relaxation could still not be fitted with a single-exponential function.

The ^{207}Pb relaxation recovery curves at 4.70 and 7.05 T cannot be uniquely fitted. We chose to fit them in two ways to make this point: (a) as a stretched-exponential function and (b) as a double-exponential function. The solid line in Figure 9 represents both fits to the data. The fits are indistinguishable. A single-exponential fit (dashed line) is indicated in Figure 9 for comparison, and it does not fit the experimental data. The stretched-exponential function[55,56]

$$M(t) = M(\infty)[1 - (1 - \cos\theta)\exp\{(-R^*t)\beta\}] \quad (2)$$

has four adjustable parameters. For these experiments, $\cos\theta \approx 0$, as mentioned above. R^* is a *characteristic* relaxation rate constant for this model, and β is the stretching parameter. We have elsewhere provided a brief review of the stretched-exponential function and the many experimental techniques that employ it,[56] and we discuss this further in the next section. This relaxation function characterizes a continuous distribution of exponential relaxation rates, and its use has not been theoretically justified by relaxation mechanisms.

The second method of fitting the data is with a double-exponential function:

$$M(t) = M_A(\infty)[1 - (1 - \cos\theta)]\exp(-R_At) + M_B(\infty)$$
$$[1 - (1 - \cos\theta)]\exp(-R_Bt) \quad (3)$$

dx.doi.org/10.1021/jp5023423 | J. Phys. Chem. C 2014, 118, 9143−9153

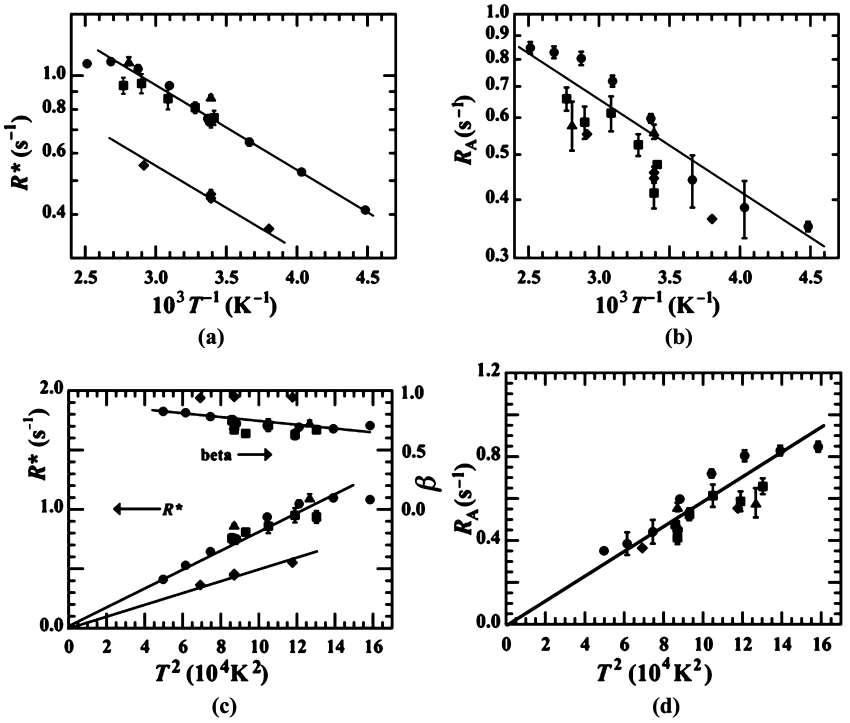

Figure 10. Various ways of presenting the ^{207}Pb NMR spin–lattice relaxation rate data in PbI_2. (a) and (c) R^*, (b) and (d) R_A measured at 4.70 T (▲) and 7.05 T (●, ■) and R at 11.75 T (♦). In (a) and (b) the rates are plotted versus inverse temperature T^{-1}, and in (c) and (d) they are plotted versus T^2. Measurements were performed at the University of California at Los Angeles (●) and at the University of Delaware (■, ♦, ▲). The stretching parameter β is also shown in (c). The straight lines are guides for the eye.

This function has five adjustable parameters to obtain a fit to the experimental data, one more than the stretched-exponential fit. Again, $\cos\theta \approx 0$. The fractional magnetization $M_A(\infty)/[M_A(\infty) + M_B(\infty)]$ relaxes with the rate constant R_A, and the fractional magnetization $M_B(\infty)/[M_A(\infty) + M_B(\infty)]$ relaxes with the rate constant R_B. Throughout the entire temperature range, the analysis shows that $M_A(\infty)/[M_A(\infty) + M_B(\infty)] \approx 0.8$ and $M_B(\infty)/[M_A(\infty) + M_B(\infty)] \approx 0.2$, almost independent of temperature.

Figure 10 shows the temperature dependence of the lead relaxation parameters by the two fitting methods. The four parts of Figure 10 show the relaxation rates R^* in eq 2 (Figure 10a,c) and R_A in eq 3 (Figure 10b,d) on a logarithmic scale versus T^{-1} (Figure 10a,b) and on a linear scale versus T^2 (Figure 10c,d). The values of R_B cannot be characterized with reasonable accuracy, which is not surprising since (1) R_B characterizes the relaxation of only approximately 20% of the magnetization and (2) all the parameters in a five-parameter fit have greater uncertainties since a four-parameter fit (the stretched-exponential function) works well. Indeed, the uncertainty bars in Figure 10a,c for R^* are smaller than those in Figure 10b,d for R_A. The highest temperature at which rate constants are reported is 398 K.

Two ^{207}Pb spin–lattice relaxation measurements above 400 K (423 and 448 K, not shown) indicated quite different ^{207}Pb relaxation behavior. These two measurements were adequately fitted by the stretched-exponential function, but *not* by a double-exponential function, despite the additional adjustable parameter. These two measurements are likely in the 4H or 12R polytype, and as discussed above, the sample was changed on return to room temperature. We know from our room-temperature powder X-ray diffraction of the initial sample that the low-temperature structure is the 2H polytype, but we cannot be certain which polytype dominates the high-temperature structure, as we did not examine the samples at these higher temperatures.

In contrast to the situation at 4.70 and 7.05 T, measurements of the ^{207}Pb relaxation rate at 11.75 T are exponential within experimental error and thus can be characterized by a single relaxation rate constant R. These values of R are similar to the values of R_A at 4.70 and 7.05 T when the relaxation is characterized by a double-exponential function (Figure 10b,d), but they are *not* similar to the R^* values when the relaxation is characterized by the stretched-exponential function. (Figure 10a,c).

5. DISCUSSION

5.1. ^{127}I Central-Transition Line Shapes. The iodine central-transition resonance in Figure 4 is well fitted by the line shape of a single ^{127}I nuclear spin species. The linear temperature variation of the quadrupolar coupling constant indicates that the average electric-field gradient at the iodine site varies linearly with temperature (Figure 5), consistent with the quadrupolar interaction being dynamically averaged by lattice vibrations. Similarly, the isotropic ^{127}I shift varies monotonically over this temperature range approximately linearly (Figure 6), which has been shown theoretically to be an indication of slight bond-length (and perhaps bond-angle) changes with temperature.[45]

5.2. ^{127}I Spin–Lattice Relaxation. One of the distinguishing features of PbI_2 is its conduction properties, which imply mobility of charge carriers. In the low-temperature 2H polytype (below approximately 400 K) and well into the 4H or 12R polytype at temperatures below approximately 540 K, the iodine atoms hop among vacancies.[34] The vacancies constitute about 20% of the sample,[23] but it seems likely that samples

dx.doi.org/10.1021/jp5023423 | J. Phys. Chem. C 2014, 118, 9143–9153

produced under different conditions (especially those annealed at high temperature) have different overall vacancy rates and probably different distributions of vacancies. In the higher temperature phases, at least above 540 K, lead atoms have been suggested to dominate the conduction, and at even higher temperatures, electron holes contribute to the conductivity.[34]

The hopping among vacancy sites subjects an iodine nucleus to time-dependent electric field gradients. For fast hopping on the NMR time scale, the solid-state NMR spectrum of the iodine nucleus reflects the time-averaged electric field gradient seen by the iodine nucleus. The temperature variation of the iodine quadrupolar coupling constant (Figure 5 and Table 2) reflects the fact that the hopping rate between sites is temperature-dependent. This is also seen in the dc electrical conductivity measurements.[34]

We can fit the temperature dependence of the ^{127}I relaxation rate in Figure 8 by assuming that the iodine relaxation rate is the sum of two mechanisms, (a) the van Kranendonk mechanism[57] *and* (b) a mechanism in which the rate constant is proportional to a thermally activated correlation time:

$$R = R_a + R_b = AT^2 + B\exp\left(-\frac{E}{kT}\right) \quad (4)$$

The van Kranendonk mechanism[57] has been used to explain quadrupolar relaxation (for spin $I > 1/2$) in a wide variety of solids and has a characteristic temperature dependence ($R_a \propto T^2$). This characteristic dependence is shown as the dashed line labeled R_a in Figure 8. However, at higher temperatures, the deviation from a T^2 dependence indicates the presence of the thermally activated mechanism R_b as shown as the dashed line labeled R_b in Figure 8. The fit of the experimental data to eq 4, shown as the solid line in Figure 8, gives $A = (1.5 \pm 0.2) \times 10^{-2}$ s^{-1} K^{-2}, $B = (10 \pm 8) \times 10^4$ s^{-1}, and $E = 15 \pm 4$ kJ mol^{-1}. The dependence of the rate constant R_b on temperature implies that the hopping process is in the limit where the mean time between hops, τ, is long compared with the inverse NMR frequency [i.e., $\tau \gg \omega^{-1}$, where $\omega = 2\pi(60.05$ MHz) at 7.05 T].[40] (This is further discussed below when eq 7 is presented.) This predicts that the component with relaxation rate constant R_b should be NMR frequency dependent, which is the case for most spectral density functions used to model solid-state relaxation rate data.[58,59] This should be tested in the future. The activation energy of approximately 15 kJ mol^{-1} (0.16 eV) is intermediate between the two activation energies for hopping (0.087 and 0.23 eV) reported from studies of the electrical properties.[5] The results suggest that only at sufficiently high temperature is the thermally activated mechanism competitive with the van Kranendonk mechanism. The most likely interpretation of the thermally activated mechanism is that it is associated with modulation of electric field gradients due to the hopping of iodine atoms throughout the lattice. A combination of these two relaxation mechanisms has been previously reported for ^{127}I relaxation in $Ag_xCu_{1-x}I$.[60,61] By this model, the van Kranendonk mechanism is approximately 100 times more efficient for ^{127}I in PbI_2 than it is for the $Ag_xCu_{1-x}I$ compounds, and the activation energy for the thermally activated process in PbI_2 is substantially lower than for $Ag_xCu_{1-x}I$, indicating a difference in the effectiveness of the two relaxation mechanisms in the two materials.

We note that, from a purely mathematical point of view, a product of the two terms in eq 4, rather than a sum, also fits the data in Figure 8. That is

$$R = CT^2\exp\left(\frac{-E}{kT}\right) \quad (5)$$

with $C = (3.8 \pm 0.4) \times 10^{-2}$ s^{-1} K^{-2} and $E/k = 216 \pm 34$ K (= 1.8 ± 0.3 kJ/mol = 18.6 meV) provides a fit to R versus T in Figure 8 that is indistinguishable from the fit using eq 4. This involves three adjustable parameters instead of the four adjustable parameters in eq 4. There is a mechanism that leads to this prediction,[62] but in this model E in eq 5 is the band gap and our fitted value is more than 2 orders of magnitude smaller than the ~2.5 eV band gap in PbI_2 measured by other methods.[2,3,5] We conclude, therefore, that this model is not appropriate here.

One may ask what other interactions between the 100% naturally abundant ^{127}I and the 22.6% naturally abundant ^{207}Pb atoms might produce effective ^{127}I relaxation. A calculation[63] of the direct ^{127}I–^{207}Pb dipole–dipole coupling at an internuclear distance of 0.32 nm yields[1] a dipolar interaction strength of only 154 Hz, much too small to produce an effective ^{127}I relaxation pathway through a dipole-mediated relaxation pathway for either nucleus.

5.3. ^{207}Pb Line Shapes. The ^{207}Pb line shape is a broad Gaussian, with a fwhm of 25 kHz, which only reduces to 20 kHz upon MAS at high field. A possible interaction that could broaden these lines is the scalar (indirect) coupling between nuclei.[58] Although no scalar (indirect) coupling is resolved in the ^{207}Pb line shape (Figure 2), the ^{127}I–^{207}Pb scalar coupling can be estimated by the fast-MAS method, which has been previously used to determine couplings for InP and GaAs.[17,64] The ^{207}Pb MAS spectra of polycrystalline PbI_2 acquired at 7.05 and 11.75 T are shown in Figure 2. The full width at half-height $\Delta\nu_{1/2}$ (in units of Hz) is related to the second moment M_2 by $\Delta\nu_{1/2} = [8(\ln 2)M_2]^{1/2}$. Using the full width at half-height of 20 kHz, the second moment is found to be $M_2 = 7.21 \times 10^7$ Hz^2 at 295 K. Assuming this broadening arises from ^{127}I–^{207}Pb scalar coupling, one obtains a value for the J coupling of 4.91 kHz, similar in magnitude to other ^{207}Pb scalar couplings.[64,65] This scalar interaction is over an order of magnitude larger than the heteronuclear dipolar interaction of 154 Hz. The small change in the half-width of the ^{207}Pb resonance upon spinning (25 kHz versus 20 kHz) is consistent with the scalar coupling being the dominant interaction that affects the line width.

5.4. ^{207}Pb Spin–Lattice Relaxation. The ^{207}Pb spin–lattice relaxation is complicated and difficult to interpret uniquely. We distinguish between the *mathematical* fitting functions used to fit the nuclear magnetization versus time in a relaxation experiment (which results in the appropriate relaxation rate constants) and the *physical* models (and their subsequent mathematical models) used to describe (fit) the temperature dependence of the resulting relaxation rate constants.

At magnetic fields of 4.70 and 7.05 T, the relaxation is *not* exponential. The decay to equilibrium of an excited ^{207}Pb nuclear magnetization (Figure 9) at any temperature can be fit either to the sum of two exponential functions (eq 3) or to a single stretched-exponential function (eq 2), and there is no *a priori* way to determine which is the better mathematical model. At the higher magnetic field of 11.75 T, the relaxation is exponential (eq 1).

The double-exponential fits (nuclear magnetization versus time) at 4.70 and 7.05 T yield the rate constants R_A and R_B, and the temperature dependence of R_A is shown in Figure 10b,d. The stretched exponential fit yields the characteristic rate

dx.doi.org/10.1021/jp5023423 | J. Phys. Chem. C 2014, 118, 9143–9153

constant R^*, and the temperature dependence of R^* is shown in Figure 10a,c. At 11.75 T, the relaxation is exponential ($\beta \approx 1$ in eq 2), and this same single rate constant is shown in all four parts of Figure 10. In Figure 10a,c it is $R = R^*$ (when $\beta = 1$), and in Figure 10b,d we associate this single-exponential rate constant R (at 11.75 T) with R_A (at 4.70 and 7.05 T). That the relaxation is exponential at 11.75 T and not exponential at 4.70 and 7.05 T is difficult to understand, and further work is needed to rationalize this observation. More interesting perhaps is that when we associate R at 11.75 T with R^* at the two lower fields, there is a magnetic field (NMR frequency) dependence to the relaxation rates (Figure 10a,c), but when we associate R at 11.75 T with R_A at the two lower fields, there is, to within experimental uncertainty, no magnetic field dependence (Figure 10b,d). This is perhaps a reminder that the stretched exponential R^* cannot be modeled in any meaningful way. It is simply a convenient parametrization of nonexponential relaxation. Its main attraction is that it requires only one parameter more than needed to parametrize exponential relaxation.

The stretched-exponential function suggests a continuous distribution of relaxation rates. The parameter R^* is "the characteristic relaxation rate", and the parameter $0 < \beta < 1$ is the "stretching factor". The parameter β is shown in Figure 10c. At the lower magnetic fields $\beta \approx 0.7$ and at 11.75 T, $\beta \approx 1$ (i.e., exponential relaxation). It is not straightforward to relate the parameters R^* and β to the dynamics. Much effort has gone into determining a distribution of exponential relaxation rates that gives the stretched exponential.[66,67] The best one can do is to relate R^* to a distribution function describing the fraction of relaxors with (an exponential) relaxation rate below R^* and the fraction above R^*. R^* should *not* be called the average relaxation rate. But even then, these distribution functions depend on β. The precise meaning of β as a general parameter is even less clear, though the smaller the value of β, the greater the (unknown) distribution of relaxation rates. The fact that β at the lower magnetic fields is very different from its value at 11.75 T makes relating R^* in the two cases problematic.

The double-exponential fits, on the other hand, have a clear physical interpretation. At 4.70 and 7.05 T, the double-exponential analysis (Figure 10b,d) gives a 0.8:0.2 ratio of the fractional magnetizations associated with R_A and R_B, respectively, and this ratio is approximately independent of temperature. This suggests that these regions of different relaxation efficiency may be correlated with the 80/20 ratio of regions without and with vacancies.

The temperature dependences of both R_A and R^* can be fitted with two, very different, *physical* models: a Raman-like mechanism or a thermally activated mechanism. The Raman-like mechanism (as applied to R^* in Figure 10c or to R_A in Figure 10d) is a lattice-vibration-based relaxation mechanism, as has reported for spin-1/2 nuclei like ^{119}Sn, ^{207}Pb, ^{203,205}Tl, and ^{129}Xe in the solid state.[68−74] In the case of spin-1/2 nuclei, the mechanism involves the modulation of an interaction similar to the spin-rotation mechanism.[71] For ^{119}Sn relaxation in α-SnF_2, the analysis also showed contributions of a thermally activated mechanism that becomes dominant at the higher temperatures,[68] like the ^{127}I relaxation results discussed above. A signature of this Raman-like mechanism is that the relaxation is independent of magnetic field (NMR frequency) and proportional to T^2:

$$R = FT^2 \tag{6}$$

Although this form is the same as the first term in eq 4, we distinguish between the van Kranendonk mechanism for spin $I > 1/2$ nuclei like ^{127}I (eq 4) and the mechanism presented in eq 6 for spin $I = 1/2$ nuclei like ^{207}Pb. The R^* versus T^2 plot in Figure 10c shows that the rates are NMR frequency (magnetic field) dependent if the single exponential rate R at 11.75 T is associated with the stretched exponential R^* at 4.70 and 7.05 T. *If this is the case, then this model is ruled out.*

The plot of R_A (with R at 11.75 T associated with R_A) versus T^2 in Figure 10d does seem field-independent, but there is a great deal of scatter. The line in Figure 10d gives F in eq 6 as $F = (6 \pm 1) \times 10^{-6}$ s^{-1} K^{-2}. This is the same order of magnitude as $(1.33 \pm 0.03) \times 10^{-6}$ s^{-1} K^{-2} in $Pb(NO_3)_2$,[69,72] $(1.18 \pm 0.07) \times 10^{-6}$ s^{-1} K^{-2} in $PbCl_2$,[70] and $(2.25 \pm 0.08) \times 10^{-6}$ s^{-1} K^{-2} in $PbMoO_4$.[70] In $Pb(NO_3)_2$, $PbCl_2$, and $PbMoO_4$, the relaxation is strictly exponential, there are no phase changes, the relaxation is not sample-dependent, and fitting the data is straightforward. As such, the uncertainties on F are quite small as opposed to the ∼15% uncertainty we quote for PbI_2.

The *other* way to interpret the temperature dependence of the relaxation rates in terms of a *physical* model is that there is a thermally activated mechanism involved, as shown in Figure 10a,b. This involves a class of models discussed below and assumes only that there is a correlation time τ that characterizes the mean times between changes in the local magnetic field in the vicinity of the ^{207}Pb nucleus. In this case, a negative slope of the ln R versus T^{-1} plots implies a thermally activated process in the slow-motion regime ($\tau \gg \omega^{-1}$)[58,59]

$$R = D\tau^{-1} = D{\tau_0}^{-1} \exp\left(-\frac{E}{kT}\right) \tag{7}$$

where R means R^* or R_A at 4.70 and 7.05 T or just R at 11.75 T and where the correlation time τ in eq 7, which we assume to be closely related to the mean time between iodine ion hops, is much greater than the inverse NMR angular frequency. This is the same reasoning used in producing the second part of eq 4. It is difficult to know what the frequency dependence should be, but in a random hopping model[58] one would expect a Bloembergen−Purcell−Pound (or Poisson or Debye) frequency dependence with $R \propto \omega^{-2}$.[58,59] Although the ion hopping is probably not isotropic in the highly anisotropic structure of PbI_2, one would still generally expect some magnetic field dependence. The appropriate algebraic form of R versus ω could be determined if one could obtain data at much higher temperature and see the transition from the slow motion region ($\tau \gg \omega^{-1}$) to the fast motion region ($\tau \ll \omega^{-1}$), but this is not possible since there are polytype phase transitions at temperatures higher than we show in Figure 10. Although it seems that, roughly, the relaxation rate constant R_A at these two low fields is field-independent, there is too much scatter in the data to state this definitively. The relaxation rate, R_B (not shown), for the efficient process is determined with very large uncertainties, so one cannot make any statement about it, except to say that it is larger than R_A, as would be expected if it corresponds to nuclei in regions with large numbers of vacancies. The data of Figure 10b (R_A versus T^{-1} which has considerable scatter) gives an activation energy in eq 7 of $E = 4 \pm 1$ kJ/mol.

There are many different *specific* interactions whose modulation by the iodine-ion hopping could affect a spin-1/2 nucleus like ^{207}Pb and be responsible for the thermally activated mechanism discussed above.[49] The line shapes give no indication of large ^{207}Pb chemical-shielding anisotropy, so it is

dx.doi.org/10.1021/jp5023423 | J. Phys. Chem. C 2014, 118, 9143−9153

unlikely that the chemical-shift-anisotropy mechanism provides a sufficiently strong contribution to relaxation. The estimated dipolar couplings between ^{127}I and ^{207}Pb are too small to account for the width of the ^{207}Pb lines, so it is also unlikely that the ^{207}Pb−^{127}I dipolar couplings provide a sufficiently strong relaxation mechanism to be dominant. The remaining interaction is the scalar coupling between ^{127}I and ^{207}Pb, and we propose that this interaction is what might induce relaxation of these ^{207}Pb spins. However, this proposal requires further investigation.

6. CONCLUSIONS

Lead iodide (PbI_2) has a crystal structure with a significant number of vacancies. In one studied sample, approximately 20% of the iodine sites were vacant, while the PbI_2 stoichiometry was maintained.[23] The variable vacancy amounts make lead iodide ideal for many potentially important applications, as outlined in the second section of this paper because one can tune the properties of the material by the number of vacancies created. The material is a reasonably good ionic conductor below approximately 400 K, with the iodine atoms carrying the charge.

The ^{207}Pb spin−lattice relaxation of the 2H polytype of PbI_2 below 400 K at 4.70 and 7.05 T can be characterized by a double-exponential function, suggesting two separately relaxing regions (with roughly a 4:1 ratio), although one can also fit the data with a stretched-exponential function, suggesting a distribution of relaxing regions. At 11.75 T, the relaxation of ^{207}Pb is close to exponential, implying that one uniformly relaxing region is detected. Because of the similarity in magnitude, we associate this single relaxation rate with the less efficient relaxation rate found at lower magnetic fields. The ^{207}Pb MAS spectrum of PbI_2 at 11.75 T is well-modeled by the sum of two Gaussian lines in the ratio of 4:1, whereas at 4.70 and 7.05 T, the spectrum is a single Gaussian function under MAS, presumably because the line shape does not narrow sufficiently to resolve the two separate components. The physical mechanism for the ^{207}Pb relaxation (spin $I = 1/2$) may be a spin-rotation interaction modulated by lattice vibrations. On the other hand, it may be a thermally induced ^{207}Pb−^{127}I scalar interaction modulated by iodine ion hopping. The iodine hopping may also affect the lattice vibrations in that they may be different in vacancy and no-vacancy regions of the sample. So, the two mechanisms might be related.

A phase transition in the range 400−420 K (probably to the 4H or 12R polytype) is seen as a discontinuity in the temperature dependence of the ^{207}Pb relaxation rates, but the line shapes seem to be continuous through this transition. Our "observation" of this phase transition is based on only two relaxation rate measurements above 400 K, but more significantly, it is also based on the fact that when samples taken to temperatures above 400 K are returned to room temperature, the relaxation rates differ significantly when compared to measurements at room temperature in samples that had never been taken above 400 K. This observation is consistent with reports of phase transitions in this temperature range.[23,25]

The ^{127}I chemical shielding and quadrupolar coupling, both determined from the ^{127}I solid-state NMR spectra, are linearly dependent on temperature. The spin−lattice relaxation of the central transition in the ^{127}I NMR spectrum is very efficient, and the dependence of R on temperature shows that, at temperatures below approximately 300 K, the ^{127}I spin−lattice relaxation is dominated by a lattice-vibration-induced modulation of electric field gradients, the van Kranendonk mechanism. At temperatures above approximately 300 K, a second, thermally activated mechanism also affects the ^{127}I relaxation rate. This mechanism probably arises from the random hopping of the iodine ions. This hopping produces relaxation to compete with the van Kranendonk mechanism.

The spectroscopic and relaxation results for ^{207}Pb and ^{127}I provide a picture of the state of PbI_2 that is generally in agreement with the results of other measurements but, in principle, at least, provides more detailed atomic-level information. Further studies at several NMR frequencies (magnetic fields) on PbI_2 samples whose thermal histories are very carefully controlled will help to elucidate some of the issues raised in the work.

AUTHOR INFORMATION

Corresponding Author

*Tel +1 (302) 831-2726; e-mail dybowski@udel.edu (C.D.).

Notes

The authors declare no competing financial interest.

ACKNOWLEDGMENTS

This material is based on work supported by the National Science Foundation under Equipment Grant # DMR-9975975. C.D. acknowledges support of NMR studies by the National Science Foundation under Grants CHE-0411790 and CHE-0956006. P.A.B. acknowledges the support of the National Science Foundation under Grant CHE-0411907.

REFERENCES

(1) Beckmann, P. A. A Review of Polytypism in Lead Iodide. *Cryst. Res. Technol.* **2010**, *45*, 455−460.

(2) Ando, M.; Yazaki, M.; Katayama, I.; Ichida, H.; Wakaiki, S.; Kanematsu, Y.; Takeda, J. Photoluminescence Dynamics Due to Biexcitons and Exciton-Exciton Scattering in the Layered-Type Semiconductor PbI_2. *J. Phys. Rev. B* **2012**, *86*, 155206 1−6..

(3) Hassan, M. A.; Jafar, M. M.; Matuchova, M.; Bulos, B. N. An Experimental Evidence of Some Lead Iodide Polytypes Compatible with the Dielectric Functions Model. *J. Appl. Sci.* **2010**, *10*, 3367−3373.

(4) Zhu, X. H.; Wei, Z. R.; Jin, Y. R.; Xiang, A. P. Growth and Characterization of a PbI_2 Single Crystal Used for Gamma Ray Detectors. *Cryst. Res. Technol.* **2007**, *42*, 456−459.

(5) Hassan, M. A.; Jafar, M. M. A. Frequency Dependence of Loss Tangent of Thermally Annealed Undoped Lead Iodide Crystals in the Dark. *Nucl. Instrum. Methods Phys. Res., Sect. A* **2006**, *566*, 526−535.

(6) Sengupta, A.; Jiang, B.; Mandal, K. C.; Zhang, J. Z. Ultrafast Electronic Relaxation Dynamics in PbI_2 Semiconductor Colloidal Nanoparticles: A Femtosecond Transient Absorption Study. *J. Phys. Chem. B* **1999**, *103*, 3128−3137.

(7) Baltog, I.; Piticu, I.; Constantinescu, M.; Ghita, G.; Ghita, L. Optical Investigations of PbI_2 Single Crystals after Thermal Treatment. *Phys. Status Solidi A* **1979**, *52*, 103−110.

(8) Baibarac, M.; Baltog, I.; Lefrant, S. Photoluminescence and Raman Spectroscopy Studies on Polyaniline/PbI_2 Composite. *J. Solid State Chem.* **2009**, *182*, 827−835.

(9) Baltog, I.; Baibarac, M.; Lefrant, S. Quantum Well Effect in Bulk PbI_2 Crystals Revealed by the Anisotropy of Photoluminescence and Raman Spectra. *J. Phys.: Condens. Matter* **2009**, *21*, 025507-1−025507-9.

(10) Kasi, G. K.; Dollahon, N. R.; Ahmadi, T. S. Fabrication and Characterization of Solid PbI_2 Nanocrystals. *J. Phys. D: Appl. Phys.* **2007**, *40*, 1778−1783.

(11) Novosad, I. S.; Novosad, S. S.; Bordun, O. M.; Pashuk, I. P. Thermally Stimulated and Photoinduced Depolarization Processes in PbI_2 Crystals. *Inorg. Mater.* **2006**, *42*, 226−230.
(12) Preda, N.; Mihut, L.; Baibarac, M.; Baltog, I.; Lefrant, S. A Distinctive Signature in the Raman and Photoluminescence Spectra of Intercalated PbI_2. *J. Phys.: Condens. Matter* **2006**, *18*, 8899−8912.
(13) Ma, D.; Zhang, W.; Zhang, R.; Zhang, M.; Xi, G.; Qian, Y. A Facile Hydrothermal Synthesis Route to Single-Crystalline Lead Iodide Nanobelts and Nanobelt Bundles. *J. Nanosci. Nanotechnol.* **2005**, *5*, 810−813.
(14) Ponpon, J. P.; Amann, M. Thermally Stimulated Current Measurements on Evaporated PbI_2 Layers. *Phys. Status Solidi A* **2003**, *198*, 150−155.
(15) Bouad, N.; Chapon, L.; Marin-Ayral, R.-M.; Bouree-Vigneron, F.; Tedenac, J.-C. Neutron Powder Diffraction Study of Strain and Crystallite Size in Mechanically Alloyed PbTe. *J. Solid State Chem.* **2003**, *173*, 189−195.
(16) Novosad, S. S.; Novosad, I. S.; Matviishin, I. M. Luminescence and Photosensitivity of PbI_2 Crystals. *Inorg. Mater.* **2002**, *38*, 1058−1062.
(17) Tomaselli, M.; deGraw, D.; Yarger, J. L.; Augustine, M. P.; Pines, A. Scalar and Anisotropic *J* Interactions in Undoped InP: A Triple-Resonance NMR Study. *Phys. Rev. B* **1998**, *58*, 8627−8633.
(18) Lifshitz, E.; Bykov, L.; Yassen, M.; Chen-Esterlit, Z. The Investigation of Donor and Acceptor States in Nanoparticles of the Layered Semiconductor PbI_2. *Chem. Phys. Lett.* **1997**, *273*, 381−388.
(19) Chang, Y.-C.; James, R. B. Phonon Dispersion and Polar-Optical Scattering in 2H PbI_2. *Phys. Rev. B* **1997**, *55*, 8219−8225.
(20) Buontempo, U.; Di Cicco, A.; Filipponi, A.; Nardone, M.; Postorino, P. Determination of the I_2 Bond Length Distribution in Liquid, Solid, and Solution, by Extended X-ray Absorption and Fine Structure Spectroscopy. *J. Chem. Phys.* **1997**, *107*, 5720−5726.
(21) Mu, R.; Tung, Y. S.; Ueda, A.; Henderon, D. O. Chemical and Size Characterization of Layered Lead Iodide Quantum Dots via Optical Spectroscopy and Atomic Force Microscopy. *J. Phys. Chem.* **1996**, *100*, 19927−19932.
(22) Bibik, V. A.; Davydova, N. A. Donor-Acceptor Emission in PbI_2 Crystals. *Phys. Status Solidi A* **1991**, *126*, K191−K196.
(23) Palosz, B.; Steurer, W.; Schulz, H. The Structure of PbI_2 Polytypes 2H and 4H: A Study of the 2H−4H Transition. *J. Phys.: Condens. Matter* **1990**, *2*, 5285−5295.
(24) Nizam, M.; Allavena, M.; Bouteiller, Y.; Suits, B. H.; White, D. NMR Chemical Shifts and the Electronic Structure of Lead in Lead Halides. *J. Magn. Reson.* **1989**, *82*, 441−453.
(25) Salje, E.; Palosz, B.; Wruck, B. *In Situ* Observation of the Polytypic Phase Transition 2H−12R in PbI_2: Investigations of the Thermodynamic, Structural, and Dielectric Properties. *J. Phys. C: Solid State Phys.* **1987**, *20*, 4077−4096.
(26) Sandroff, C. J.; Kelty, S. P.; Hwang, D. M. Clusters in Solution: Growth and Optical Properties of Layered Semiconductors with Hexagonal and Honeycombed Structures. *J. Chem. Phys.* **1986**, *85*, 5337−5340.
(27) Sandroff, C. J.; Hwang, D. M.; Chung, W. M. Carrier Confinement and Special Crystallite Dimensions in Layered Semiconductor Colloids. *Phys. Rev. B* **1986**, *33*, 5953−5955.
(28) Schoonman, J.; Wolfert, A.; Untereker, D. F. Hebb−Wagner Polarization of PbI_2 with Conducting Iodine Electrodes. *Solid State Ionics* **1983**, *11*, 187−193.
(29) Yadav, D. P.; Acharya, H. N.; Rao, K. V. Effect of Quenching and X-ray Iradiation on the Dielectric Properties of PbI_2 Single Crystals. *Phys. Status Solidi A* **1981**, *64*, 413−417.
(30) Hagihara, T.; Nagata, S.; Ayai, N.; Ayai, N. Temperature Dependence of the Photovoltaic Effect in PbI_2 Single Crystals. *Jpn. J. Appl. Phys.* **1981**, *20*, 1003−1004.
(31) Minagawa, T. X-ray Study of the 2H−12R Structural Transformation in PbI_2. *Phys. Soc. Jpn.* **1981**, *50*, 902−906.
(32) Adduci, F.; Baldassarre, L.; Maggipinto, G.; Minafra, A.; Levy, F. Defect Levels in PbI_2 by TSC Measurements. *Phys. Status Solidi A* **1979**, *52*, K173−K178.
(33) Minagawa, T. Five New Polytypes and Polytypic Change in PbI_2. *J. Appl. Crystallogr.* **1979**, *12*, 57−59.
(34) Lingras, A. P.; Simkovich, G. Electrochemical Studies on Lead Iodide. *J. Phys. Chem. Solids* **1978**, *39*, 1225−129.
(35) Dorner, B.; Ghosh, R. E.; Harbeke, G. Phonon Dispersion in the Layered Compound PbI_2. *Phys. Status Solidi B* **1976**, *78*, 655−659.
(36) Tubbs, M. R. The Optical Properties and Chemical Decomposition of Halides with Layer Structures. 1. Crystal Structures, Optical Properties, and Electronic Structure. *Phys. Status Solidi B* **1972**, *49*, 11−50.
(37) Mitchell, R. S. Structural Polytypism of Lead Iodide and Its Relationship to Screw Dislocations. *Z. Kristallogr.* **1959**, *111*, 372−384.
(38) Tilley, R. *Crystals and Crystal Structures*; Wiley: Chichester, 2006.
(39) Mehrotra, V.; Lombardo, S.; Thompson, M. O.; Giannelis, E. P. Optical and Structural Effects of Aniline Intercalation in PbL_2. *Phys. Rev. B* **1991**, *44*, 5786−5790.
(40) Kimmich, R. *NMR Tomography, Diffusometry, Relaxometry*; Springer-Verlag: Berlin, 1997.
(41) Dybowski, C.; Smith, M. L.; Hepp, M. A.; Gaffney, E. J.; Neue, G.; Perry, D. L. ^{207}Pb NMR Chemical Shift Tensors of the Lead (II) Halides and Lead (II) Hydroxyhalides. *Appl. Spectrosc.* **1998**, *52*, 426−429.
(42) Dmitrenko, O.; Bai, S.; Dybowski, C. Prediction of ^{207}Pb NMR Parameters for the Solid Ionic Lead (II) Halides Using the Relativistic ZORA-DFT Formalism. Comparison with the Lead-Containing Molecular Systems. *Solid State Nucl. Magn. Reson.* **2008**, *34*, 186−190.
(43) Jokisaari, J.; Järvinen, S.; Autschbach, J.; Ziegler, T. ^{199}Hg Shielding Tensor in Methylmercury Halides: NMR Experiments and ZORA DFT Calculations. *J. Phys. Chem. A* **2002**, *106*, 9313−9318.
(44) Wolff, S. K.; Ziegler, T.; van Lenthe, E.; Baerends, E. J. Density Functional Calculations of Nuclear Magnetic Shielding Using the Zeroth-Order Regular Approximation (ZORA) for Relativistic Effects: ZORA Nuclear Magnetic Resonance. *J. Chem. Phys.* **1999**, *110*, 7689−7698.
(45) Dmitrenko, O.; Bai, S.; Beckmann, P. A.; van Bramer, S.; Vega, A. J.; Dybowski, C. The Relationship Between ^{207}Pb Chemical Shift and Solid State Structure in Pb(II) Compounds. *J. Phys. Chem. A* **2008**, *112*, 3046−3052.
(46) Harris, R. K.; Becker, E. D.; De Menezes, S. M. C.; Goodfellow, R.; Granger, P. NMR Nomenclature. Nuclear Spin Properties and Conventions for Chemical Shifts (IUPAC Recommendations 2011). *Pure Appl. Chem.* **2001**, *73*, 1795−1818.
(47) Kunwar, A. C.; Turner, G. L.; Oldfield, E. Solid-State Spin-Echo Fourier Transform NMR of ^{39}K and ^{67}Zn Salts at High Field. *J. Magn. Reson.* **1986**, *69*, 124−127.
(48) Widdifield, C. M.; Bryce, D. L. Solid-state ^{127}I NMR and GIPAW DFT Study of Metal Iodides and Their Hydrates: Structure, Symmetry, and Higher-Order Quadrupole-Induced Effects. *J. Phys. Chem. A* **2010**, *114*, 10810−10823.
(49) Bakhmutov, V. I. *Practical NMR Relaxation for Chemists*; John Wiley & Sons: Chichester, England, 2004.
(50) Beckmann, P. A.; Dybowski, C. A Thermometer for Non-Spinning Solid-State NMR Spectroscopy. *J. Magn. Reson.* **2000**, *146*, 379−380.
(51) Autschbach, J.; Ziegler, T. Solvent Effects on Heavy Atom Nuclear Spin-Spin Coupling Constants: A Theoretical Study of Hg−C and Pt−P Couplings. *J. Am. Chem. Soc.* **2001**, *123*, 3341−3349.
(52) Dybowski, C.; Neue, G. Solid State ^{207}Pb NMR Spectroscopy. *Prog. Nucl. Magn. Reson. Spectrosc.* **2002**, *41*, 153−170.
(53) The simulation was performed with the solids simulation package ("solaguide") in the TopSpin (Version 2.1) NMR software program from Bruker BioSpin.
(54) Yesinowski, J. P. Solid-State NMR of Inorganic Semiconductors. In *Solid State NMR*; Chan, J. C., Ed.; Topics in Current Chemistry; Springer: Heidelberg, 2012; pp 229−312.
(55) Kohlrausch, R. Theorie des Elektrischen Rückstandes in der Leidener Flasche (Theory of Electrical Residue in a Leiden Jar). *Ann. Phys. Chem.* **1854**, *91*, 179−213.

(56) Beckmann, P. A.; Schneider, E. Methyl Group Rotation, H-1 Spin-lattice Relaxation in an Organic Solid, and the Analysis of Nonexponential Relaxation. *J. Chem. Phys.* **2012**, *136*, 054508-1−054508-9.
(57) van Kranendonk, J. Theory of Quadrupolar Spin-lattice Relaxation. *Physica (Amsterdam)* **1954**, *20*, 781−800.
(58) Abragam, A. *The Principles of Nuclear Magnetism*; Oxford University Press: Oxford, 1961.
(59) Beckmann, P. A. Spectral Densities and Nuclear-Spin Relaxation in Solids. *Phys. Rep.* **1988**, *171*, 85−128.
(60) Mizuno, M.; Iijima, T.; Kimura, J.; Endo, K.; Suhara, M. Solid ^{63}Cu and ^{127}I NMR Studies of Dynamical Structure in the γ-Phase of $Ag_xCu_{(1-x)}I$ (x = 0.05 − 0.40). *J. Mol. Struct.* **2002**, *603*, 239−244.
(61) Mizuno, M.; Hirai, A.; Matsuzawa, H.; Endo, K.; Suhara, M. Dynamical Structure of $Ag_xCu_{(1-x)}I$ (x = 0.99 − 0.80) in Ionic and Superionic Phases Studied by Solid ^{63}Cu and ^{127}I NMR Spin-Lattice Relaxation Time Measurements. *Phys. Chem. Chem. Phys.* **2001**, *3*, 107−110.
(62) Wolf, D. *Spin-Temperature and Nuclear-Spin Relaxation in Matter*; Clarendon: Oxford, 1979; pp 398−402.
(63) Levitt, M. H. *Spin Dynamics, Basics of Nuclear Magnetic Resonance*; John Wiley & Sons: Chichester, 2001; pp 203−204.
(64) Potter, L. D.; Wu, Y. NMR Measurements of Homonuclear Indirect Couplings in GaAs. *J. Magn. Reson., Ser. A* **1995**, *116*, 107−112.
(65) Kennedy, J. D.; McFarlane, W.; Wrackmeyer, B. Indirect Nucelar Spin-Spin Coupling of Lead-207 to Other Magnetic Nuclei. *Inorg. Chem.* **1976**, *15*, 1299−1302.
(66) Helfand, E. On Inversion of the Williams-Watts Function for Large Relaxation Times. *J. Chem. Phys.* **1983**, *78*, 1931−1934.
(67) Johnston, D. C. Stretched Exponential Relaxation Arising from a Continuous Sum of Exponential Decays. *Phys. Rev. B* **2006**, *74*, 184430-1−184430-7.
(68) Neue, G.; Bai, S.; Taylor, R. E.; Beckmann, P. A.; Vega, A. J.; Dybowski, C. ^{119}Sn Spin-Lattice Relaxation in α-SnF_2. *Phys. Rev. B* **2009**, *79*, 214302-1−214302-5.
(69) de Castro, P.; Maher, C. A.; Vold, R. L.; Hoatson, G. L. High Field ^{207}Pb Spin-lattice Relaxation in Solid Lead Nitrate and Lead Molybdate. *J. Chem. Phys.* **2008**, *128*, 052310-1−052310-6.
(70) Beckmann, P. A.; Bai, S.; Vega, A. J.; Dybowski, C. ^{207}Pb Spin-Lattice Relaxation in Solid $PbMoO_4$ and $PbCl_2$. *Phys. Rev. B* **2006**, *74*, 214421-1−214421-4.
(71) Vega, A. J.; Beckmann, P. A.; Bai, S.; Dybowski, C. Spin-Lattice Relaxation of Heavy Spin-1/2 Nuclei in Diamagnetic Solids. A Raman Process Mediated by the Spin-Rotation Interaction. *Phys. Rev. B* **2006**, *74*, 214420-1−214420-16.
(72) Grutzner, J. B.; Stewart, K. W.; Wasylilshen, R. E.; Lumsden, M. D.; Dybowski, C.; Beckmann, P. A. A New Mechanism for Spin-Lattice Relaxation of Heavy Nuclei in the Solid State: ^{207}Pb Relaxation in Lead Nitrate. *J. Am. Chem. Soc.* **2001**, *123*, 7094−7100.
(73) Fitzgerald, R. J.; Gatzke, M.; Fox, D. X.; Cates, D. G.; Happer, W. ^{129}Xe Spin Relaxation in Frozen Xenon. *Phys. Rev. B* **1999**, *59*, 8795−8811.
(74) Villa, M.; Avogadro, A. Indirect Interactions and Nuclear Relaxation $TlNO_3$. *Phys. Status Solidi B* **1976**, *75*, 179−188.